System Simulation for M-Sequence Radar Sensors

Markus Robens, Ralf Wunderlich and Stefan Heinen
Integrated Analog Circuits and RF Systems
RWTH Aachen University
Aachen, Germany
ias@rwth-aachen.de

Jürgen Sachs
Electronic Measurement Research Lab
Ilmenau University of Technology
Ilmenau, Germany
juergen.sachs@tu-ilmenau.de

***Abstract*—Capabilities of M-sequence radar front-ends have been shown in the past. For further system enhancement, specifications of constituent components can be re-aligned using system simulation. In this article, we want to present a system simulation setup for Agilent's Advanced Design System (ADS) which allows us to assess the impact of individual components on typical radar parameters. The latter characterize the performance of the overall system and it is their optimization which is targeted. For this purpose, new ADS stars, i.e. components for the (timed) synchronous dataflow (TSDF) simulator, have been implemented. Appropriate antenna models have been identified from literature and the signal deformations they impose are clearly visible from the simulated impulse response. Thus, simulations help to determine the antenna type suitable for the application. Due to the multiple signal domain simulation ability of ADS Ptolemy, it can be switched from a pure model based simulation to a transient-TSDF co-simulation during the design process. Using an appropriate channel model, such simulations provide a good estimate of real system performance right in advance to the actual component implementation and they help to keep track of real components agreement with the predicted behavior. Thus, a fair amount of flexibility is added in the design process compared to the former real-circuit component based approach.**

***Keywords*—M-sequence radar system; system simulation; system parameters; co-simulation**

I. Introduction

Application of ultra-wideband (UWB) sensor devices has been reported for a couple of localization tasks. Those tasks profit from high range resolution and range accuracy, which results from the large bandwidth of excitation signals in UWB systems. Range resolution characterizes the ability to distinguish adjacent scatterers or interfaces in range direction. According to narrowband radar theory, this quantity is directly related to the inverse of bandwidth. Range accuracy, i.e. the capability to precisely detect the position of a certain interface, in addition is affected by noise. Though, according to [1], the analytic models used to describe these relationships require some refinement when UWB signals are focused, the underlying principles remain valid even in the UWB case.

To a certain extent, UWB signals are also robust against multipath propagation. In [2], for example, time of arrival estimation for signals in a multipath environment is examined and compared to other time of arrival estimation techniques. At a reasonable signal to noise ratio (SNR), estimation techniques proposed in this publication perform well under line-of-sight and non-line-of-sight conditions while they require only low computational complexity.

Some applications take advantage of lower frequencies, which are part of the UWB stimulation spectrum. Related signal portions might enter or pass through non-metallic materials and thus provide information on the material itself or the area behind. In [3], through-wall detection is demonstrated for one of the sensor nodes, which are applied for multiple target detection by computational efficient real-time algorithms.

Driven by the requirements of a home-entertainment system, in which the user position is determined to adapt the sound for optimal listening experience, in [4] the dynamic range of a UWB device is identified as another critical system parameter. For this purpose, a sensor configuration with one transmit and four receive channels (channel sounder) is employed. Using different arrangements of the named components, it has been shown, that the dynamic range of the channel sounder is critical in view of the ability to detect a listeners position, because multipath components might mask the desired signal. If sufficient dynamic range is provided, it is possible to remove those (static) undesired signals by a background subtraction algorithm as proposed in [4]. As another prerequisite, the main peak of the impulse response function (IRF) should exhibit only small temporal jitter. If jitter gets to large, samples of static objects might be misinterpreted as those of moving objects. In this case, background subtraction fails.

The M-sequence channel sounder used in [4], or variants of it as used in [1], [3], have also been applied in other fields like ground penetrating radar and medical applications (see [5]). The requirement of large dynamic range is common to all those problems, because the desired signals (i.e. reflections from the listener, land mines or cancerous tissue) will be obscured by strong undesired responses (e.g. from the direct path, the air-to-ground or the air-to-skin interface). The same is true with respect to IRF jitter, since accurate interface positions need to be determined in all cases to avoid masking of small signals while estimates of interface-related interfering signals are removed from the measurement data. Low IRF jitter, however, not only is important for this purpose, but it also enables the detection of interfaces with very high accuracy. The latter is especially important for medical applications, since very small structures or interface displacements have to be resolved in this case. In [6], for example, sub-millimeter precision using a transmit power of approximately $4\,mW$ is claimed. Results in [1] encourage even higher accuracy. Usually, all those requirements are merged into key figures,

978-1-4673-1954-6/12/$31.00 ©2012 IEEE

which are examined in the next section.

II. Key Figures

Requirements of a certain application are generally given in form of key figures. In the introduction, the importance of high real time dynamic range and high range accuracy, i.e. low IRF jitter, has already been pronounced. There are, of course, more key figures to characterize a whole system. [5] contains a good overview. Here, they are only listed for completeness:

- Range resolution δ_r
- Range accuracy Δr
- Unambiguity range R_u
- Maximum target velocity $v_{r,max}$
- Dynamic range
  - Maximum signal to noise ratio D_{max}
  - Spurious free dynamic range D_{opt}
  - Clutter free dynamic range D_{dc}
  - System performance D_{sys}

The first four items are closely related. They are linked by the (wideband) ambiguity function. As has been mentioned with respect to range accuracy in the introduction, most key figures are valid for both, narrowband as well as wideband systems. However, focusing on some of them, care should be exercised, because they might get a different flavor in the wideband case (see [1]). Thus, it is beneficial to build a demonstrator system at an early development state, to verify results gained from analytical calculations. By this approach, mutual improvement of the demonstrator and tailored key figures can be achieved. With respect to the M-sequence system, publications at [7] reflect this line of action and serve as comprehensive knowledge base. Taking advantage of reported experiences, the use of system simulation for further system enhancement is proposed. By this approach, the impact of certain components or certain component parameters on system performance can be examined directly. The value of a key figure is simulated rather than calculated by analytical expressions. While the basic system conception might still be based on analytical considerations, system simulation can be used for fast verification. In addition, system simulation offers in-depth insight into system conditions. If results are verified against the real system, regularly, system simulation can be a valuable tool in system design. A decisive advantage, which arises, is the ability to adjust impedance levels. As opposed, impedance levels in a demonstrator are fixed by the discrete components (often to $50\,\Omega$). Due to this ability, system simulation can support the transition from a discrete to an integrated solution. There are other advantages as well. System simulation can shorten design cycles and can help to ensure suitable component designs. Hence, system simulation should be included as intermediate step in the procedure reported so far.

III. System Simulation

As proposed in the previous section, a model has been developed for a baseband M-sequence system, which has been tied to the requirements of medical applications. In [8] it is discussed, in which way characteristics of UWB signals can be used to enable reliable breast cancer detection. One problem are short reflections from the skin, which may mask tumor responses. They have a similar impact as the direct path in the home-entertainment scenario of the introduction, but the non-planar geometry aggravates the situation further. In [8], also, synergetic use of UWB sensing and magnetic resonance imaging (MRI) is envisaged to detect appropriate trigger events for cardiac MRI. Those are required for motion compensation in modern high field MRI systems. In [6], this is covered in more detail and additional applications are identified. To ensure sufficient wave propagation in biological tissues during the measurements, low frequency components should be present in the sounding signal. Summarizing all requirements and following the aim to discover the full potential of the sensor principle by new application scenarios, compliance with UWB radiation rules has not been guaranteed. This does not imply any problems, as long as measurements are conducted in a screened room, but it would preclude the use of sensors for indoor scenarios. Fortunately, in [9] it is shown, that compliance with radiation rules can be achieved by inclusion of an upconversion mixer. This measure can be respected in the model. Required modifications in the real system can be guided by system simulation, since antenna models have been implemented, which give access to the maximum electrical field strength in free space. Consequently, it is easy to check mask requirements, because they are specified in terms of effective isotropic radiated power (EIPR) values.

Fig. 1 shows the block level schematic of the implemented M-sequence baseband model. Only few blocks contain additional sub-components which will be presented in the discussion that follows. First, some specifics of the Ptolemy simulator have to be mentioned. Then, overall system operation will be considered before principles and implementations of sub-blocks will be described.

ADS Ptolemy allows for the simulation of hierarchical designs, components of which may belong to different domains [10]. A mix of domains requires that a child network obeys to the semantics of the parent domain at common interface positions. Hence, two domains which are part of ADS Ptolemy as well as circuit envelope and transient simulation can be used. Synchronous Dataflow (SDF), which is part of ADS Ptolemy, is a data driven, statically scheduled domain. This means, that flow control is completely predictable at compile time. Timed Synchronous Dataflow (TSDF), the second simulation domain of ADS Ptolemy, extends this concept by the introduction of an additional (Timed) data type. Apart from the numerical data, this type contains additional attributes like time step and center frequency. A simulation then is executed in two steps: First, balancing equations are solved (scheduling) which help to determine the activation sequence of components in a second step - the data processing.

With respect to our model, especially the relation of the Ptolemy-inherent domains is of interest. Since TSDF simulation extends SDF simulation by the introduction of a data type with additional attributes, subsampling in the time domain of

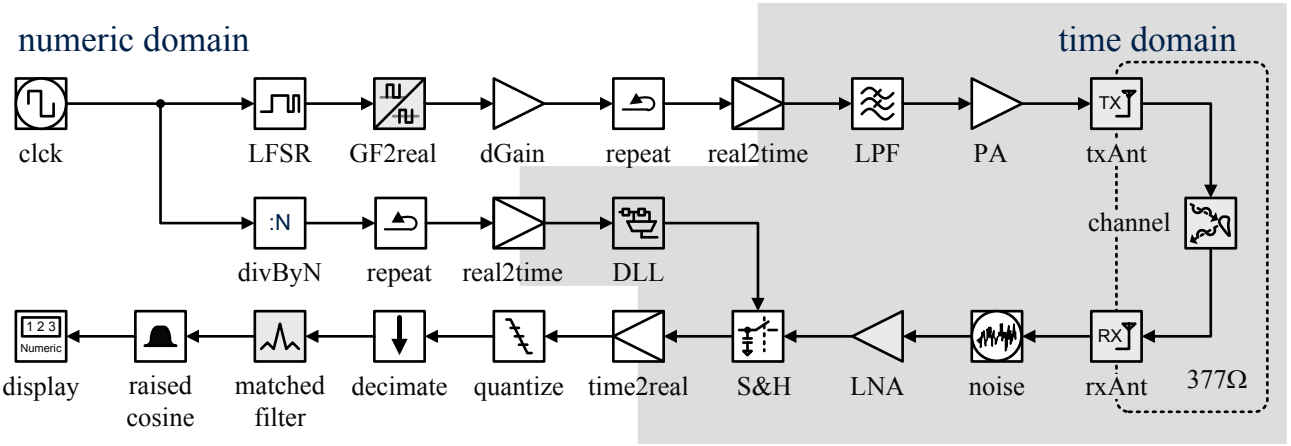

Fig. 1. Simulation setup for basic system. Gray shaded components are either newly implemented or completed by some models.

Fig. 1 just implies the generation of additional (numerical) samples with the same attributes. Similarly, since the time step used for generating an appropriately timed M-sequence is to coarse for the simulation of a timed anti-aliasing filter, samples of the M-sequence and the clock-system have to be repeated while the simulation time step is reduced. Owing to this principle, timing and the number of data samples per chip of the M-sequence are crucial aspects for the design.

After this short excursion about (T)SDF simulation and the identification of main pitfalls in the design, the simulation setup presented in Fig. 1 will be analyzed. In this setup, a pulse based clock signal (clck) of period $p = 2$ excites a linear feedback shift register (LFSR). Feedback coefficients and seed values have been selected such that an M-sequence of period $N = 511$ is generated[1]. Since the fast Walsh-Hadamard transform is used for matched filtering in the receiver, it is useful to transfer the Galois-field sequence into a sequence defined over the reals (see [11]). This is done by the GF2real component. Then, appropriate weighting (dGain) and the discussed sample repetition have to be applied in advance to the conversion into time domain (real2time) to obtain a sequence similar to that in a practical implementation. A repetition factor of $k = 16$ and a time step of $t_{ts} = 3.44\,ps$ have been selected to yield a chip duration of $t_c \approx 110\,ps$. As about 80% of the signal energy are concentrated in a signal bandwidth ranging up to $f_c/2$, i.e. half the clock frequency, limiting the spectrum to this value does not harm the M-sequence signal to much, while noise power is reduced and Nyquist-sampling at a rate of $f_s = f_c$ becomes possible. However, analog filters do not provide brick wall behavior but reveal a more soft transistion from passband to stopband. Thus, to allow for (close to) ideal interpolation in the digital domain, the equivalent sampling rate is increased in this simulation. The idea of increased equivalent sampling rate has been proposed in [12] and is enabled by the DLL component in this design (see III-A). Before the signal is 'emitted' by the transmit antenna, it is amplified by a power amplifier (PA). In the simulation, a simple model composed of memory and non-linearity mimics its behavior[2]. More important for the result of system simulation is an accurate modeling of the antennas and the signal path, because they modify signal amplitude and signal shape to a large extent. Hence, subsections III-C and III-D are devoted to these topics. As usual, thermal noise at the input of the receiver and noise properties of the low noise amplifier (LNA), specified in terms of noise figure (NF), are assumed to be the only sources of random noise in the simulation. To account for thermal noise, the AddNDensity component of ADS Ptolemy (noise) is spliced in. It allows for the specification of a noise power density, which is superimposed to the signal at this position. In the introduction, the requirement of large dynamic range for successful background subtraction has been determined, which indicates that LNA as well as analog to digital converter (ADC) are critical components in the M-sequence system. Due to its co-simulation capability, different possibilities do exist in ADS Ptolemy to accurately reflect the LNA behavior. Since we implemented different amplifier versions for this system in the past [14], [15], [16], one way would be a transient-TSDF co-simulation. This kind of simulation is supported by models of integrated components provided by IHP Microelectronics for the ADS simulator and is one reason, why ADS Ptolemy is favored over Matlab/Simulink. For verification purposes, co-simulation is an evident choice. Considering simulation time, especially in the case of jitter analysis presented later, the use of a model, which is composed of GainRF and S-parameter blocks, is a good alternative. The GainRF blocks allow for the specification of non-linearity and noise figure, while gain and frequency behavior are covered by the S-parameter block[3]. In

[1]Then, 1022 numeric samples are produced at the output of this component, because one chip of the M-sequence lasts for two numeric samples.

[2]A timed filter and the GainRF component of ADS Ptolemy are used for this purpose. Required values for gain, bandwidth and output $1\,dB$ compression point are taken from [13].

[3]For further speed enhancement, replacement of the S-parameter block by an infinite impulse response filter implementation could be an option. As in the case of UWB antennas (see III-C), frequency behavior of an UWB-LNA is characterized by a low number of resonances. Hence -by analogy- it should be possible to apply a spectral estimation technique to determine a minimal representation of the LNA.

order to generate the simulation results presented in section IV, a model of the active feedback LNA from [14] has been used. As in most UWB sensors, subsampling by a factor of M is applied in the receiver of the real system, because ADC and digital signal processing are incapable to process the receive signal at full speed. Fortunately, periodicity of the excitation signal enables the accumulation of a complete sample-set over some periods of the sequence. With respect to this scheme of data acquisition, use of an M-sequence sounding signal holds the advantage, that sampling control can be realized by a binary divider in a very stable and precise fashion [1], [5]. As discussed before, the component termed DLL is included in this simulation, to enable 'virtual oversampling' (see section III-A). After sampling and conversion from time into numeric domain (time2real) is performed, the signal is quantized according to the resolution of a real ADC [17]. Owing to a quite low resolution (4 bit), a notable amount of quantization noise is generated at this stage. Then, the number of numerical samples needs to be decimated (decimate). Caused by subsampling, repetition and the generation of the M-sequence itself, the number of numerical samples is increased compared to the number of samples in a real system (see properties of SDF/TSDF simulation). The factor $p \cdot k \cdot M$, by which the number of samples is increased, does not depend on whether virtual oversampling is applied or not, because in any case a complete sample-set is acquired before potential phase switching takes place. The 'restoration' of the numerical sample rate is an important prerequisite for impulse compression by matched filtering (matched filter), since only one sample per chip of the M-sequence is expected by this digital filter. The discussion of the matched filter in section III-B will throw some light on these relationships. The final stage of this processing element depicted in Fig. 5 also accounts for the 'virtual oversampling'. Finally, in order to simplify the estimation of jitter, an Si-interpolator is used to reconstruct a smooth time course of the IRF. This is possible, because the requirements of the sampling theorem are met - especially in the case of 'virtual oversampling'. In the simulation, a raised cosine filter with interpolation factor 16, a length of 321 and excess bandwidth 0 is used for this purpose. Table I summarizes the most important simulation parameters and settings. Next, those components will be considered for which a detailed discussion has been postponed.

A. Increased equivalent sampling rate

The idea behind this method first was sketched in [12]. In order to increase the equivalent sampling rate, sampling-sets of different signal phases are recorded subsequently. Then, data are reorganized so that samples of adjacent signal phases are also adjacent in the new, enlarged data set. The last description paraphrases data permutation which is known as perfect shuffle [18]. This versatile operation is famous in parallel processing and will be used for matched filtering excessively. For the simulations discussed here, only two different phases are used. Since in the real system -most likely- a balanced topology will be chosen for sampling control (binary divider), two phases are accessible anyway and only a fast multiplexer (and a counter) are required for phase switching. According to our experiences, implementation of a fast multiplexer should be possible. Lacking a balanced topology, the setup shown in Fig. 2 has been used for system simulation. The second delay element in this figure realizes the required phase delay while the first delay element centers the phases within the chip duration. The divider (divByN) only releases one trigger event per period of the M-Sequence and the counter (cnt) accumulates them modulo two. According to the output value (0 or 1), a multiplexer (MUX) finally selects the appropriate signal phase. In the real system as well as in simulation, data permutation as discussed in the above paragraph will be performed as part of the matched filter processing (the second perf shuff block in Fig. 5), which is treated below.

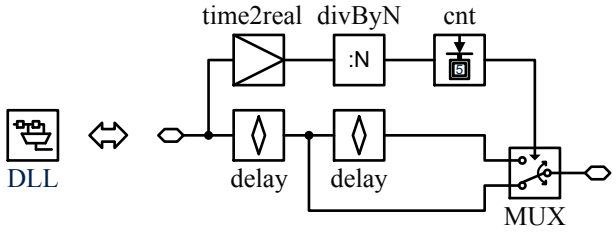

Fig. 2. Phase selection circuit.

B. Matched filter

An efficient implementation of the matched filter is a key requirement for a successful simulation of the M-sequence system. While many other components required for system simulation could be taken from some ADS libraries, components needed for the matched filter had to be implemented. They have been compiled into a new ADS library. Fortunately, processing of M-sequences is well understood and an efficient algorithm for the core of this filter has been reported in [11]. It is based on a factorization of the M-sequence matrix M using $GF(2)$ arithmetics[4]. M contains all cyclically shifted versions of the sequence:

$$M = L \cdot S. \tag{1}$$

[4]GF(2) is the finite field of integers modulo 2.

TABLE I
SIMULATION PARAMETERS

Parameter	Symbol	Value
time step	t_{ts}	$3.44\,ps$
chip duration	t_c	$110.08\,ps$
duration of a period	t_p	$56.25\,ns$
number of chips per sequence	$N = 2^n - 1$	511
sub-sampling factor	$M = 2^m$	4
virtual oversampling	O	2
repetition factor	k	16
clock period	p	2
analog filter bandwidth	BW	$4.5\,GHz$
interpolation factor	I	16
raised cosine filter length	L	321
raised cosine excess bandwidth	a	0
peak voltage at LFSR output	$V_{LFSR,p}$	$80\,mV$

It is shown, that the matrices used for factorization, L and S, have some unique properties:

- Every nonzero binary n-vector must appear as some row of L and S^T, in which $N = 2^n - 1$ is the length of sequences in M and T denotes the matrix transpose.
- They are determined by natural state-sequences of appropriate feedback shift registers, which share coefficients with the generator of M. More precisely, S contains all the states of the Fibonacci-style shift register generating the sequences of M, while L contains the states of its Galois-type equivalent. Fig. 3 illustrates their relations.

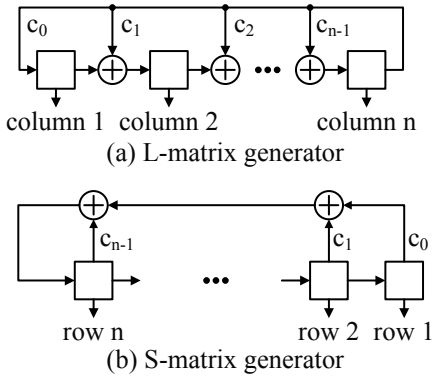

Fig. 3. Feedback generators for matrices L and S from [11].

It is known that the Walsh-Hadamard-Matrix -defined over $GF(2)$- can be factored similarly

$$H = B \cdot B^T, \tag{2}$$

in which B contains all binary n-vectors in their natural order with their decimal equivalents $0 \ldots 2^n - 1$. If L and S^T are completed by all-zero row-vectors at the top, the relation between the modified matrices $\hat{L}$ or $\hat{S}^T$ and B is just permutational:

$$\hat{L} = P_L \cdot B \qquad \hat{S}^T = P_S^T \cdot B. \tag{3}$$

Thus, matched filtering of an M-sequence sampled at Nyquist-rate can be performed by the fast Walsh-Hadamard transform (FWHT), if pre- and post-permutations according to P_S and P_L are applied. As the relation is permutational, it also holds if the FWHT is declared over the reals by substituting $0 \rightarrow +1$ and $1 \rightarrow -1$.

Matrices P_L and P_S need to be generated only once, right at the beginning of a simulation. ADS Ptolemy provides a `begin()`-method for this purpose, which is executed once - before data processing starts. The possibility to interpret n-element bitvectors as integer values in addition allows for a very efficient computation of these matrices using bitwise *C++*-operators. Our implementations thus draw upon the example given in the file `SDFscrambler.pl` from the ADS Ptolemy example directory. In fact, there is no need for an explicit matrix operation. From (3) it can be observed, that P_L and P_S^T scramble data from their natural order to an order specified by $\hat{L}$ or $\hat{S}^T$, respectively. The integer values obtained by the computation of $\hat{L}$ or $\hat{S}$ can thus be interpreted as indices specifying index manipulations which replace the matrix based permutations.

For the implementation of FWHT, *C++*-code proposed by [19] has been used. A closer look at the signal flow graph corresponding to this code reveals, that it realizes FWHT processing based on the fast Kronecker product algorithm presented in [20] in elegant manner. For shortness, this is illustrated in Fig. 4 for an example of $N = 8$.

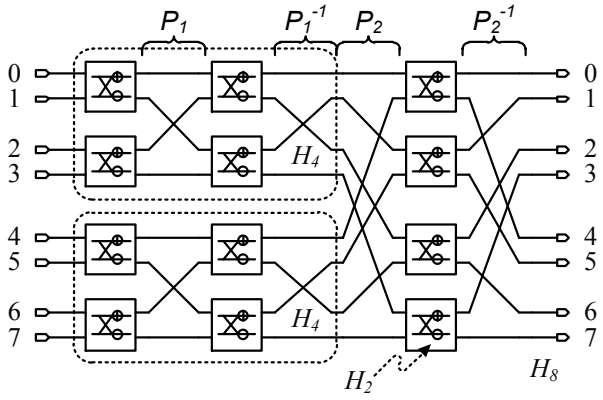

Fig. 4. FWHT processing by code of [19] denoted by the fast Kronecker product representation of [20] for $N = 8$.

As can be seen, the algorithm of [20] has to be applied recursively in order to calculate higher order Walsh-Hadamard matrices. Also interesting to note about this scheme is the fact, that in each recursion four elementary operations are involved. First, data are exposed to a first set of processing elements. Then, a perfect shuffle permutation P of appropriate order suitable for the size of the individual block is performed. In a third step, permuted data are fed into a second set of processing elements and finally another permutation P^{-1} is executed[5], which is inverse to the perfect shuffle permutation. Factorizations similar to this are reported in some publications of that time. In [21], for example, such factorization is derived based on the properties of Kronecker product and perfect shuffle operations. A closer look at P^{-1} -for example at the output of H_8- reveals that it agrees with the data permutation which occurs when data are subsampled. This means, that odd numbered samples are collected first, before even number samples are grouped together.

The last observation is remarkable, because it allows us to deal with subsampling as well as 'virtual oversampling' in a very simple manner. For the case that signal samples are acquired over several signal periods, they do arrive in distorted order according to sampling control. As a binary divider is used for this purpose, first samples with odd indices spaced 2^m positions apart are collected. Next, even numbered samples with the same spacing are accumulated and so on, until all samples of a set are gathered. However, the original sample

[5]This inverse permutation is inherent to the processing in [19], because data are processed in-place.

order has to be restored before the IRF can be calculated by the matched filter core. In order to retrieve it, we can utilize the inverse relationship of subsampling and perfect shuffle permutation. Because of this relationship, m fold application of the perfect shuffle on the gathered data set is sufficient to reconstruct the desired sequence. According to [18], the implementation of a perfect shuffle is pretty simple. Binary representations of indices from a data vector just need to be cyclically shifted m positions to the left to determine the new position of a datum after an m fold shuffle. *C++*-code for this component hence is short and simple. It works well as long as block size and data size differ at most by one which is the case for data restoration of subsampled data. However, if it is applied to realize 'virtual oversampling', things are a little bit more involved. Block and data sizes then, in general, will differ by more than one and some offset effects have to be considered, but with small changes the same principle holds. In this case, the size of the shuffle depends on the number of signal phases O, because it should comprise all related sample sets. The number of executions is given by $\log_2(O)$, which implies that O should be a power of two.

Now, all components of the matched filter from Fig. 5 have been discussed. The components indicated as core provide the IRF in the case of Nyquist-sampling and are those discussed in [11]. The component named 'perm' is used for data permutation according to P_S, 'FWHT' behaves as expected and 'perm (inv)' takes the task of P_L. The perfect shuffle to the left of the core circuit is required for data reordering after subsampling, while the perfect shuffle to the right can be used to realize 'virtual oversampling'.

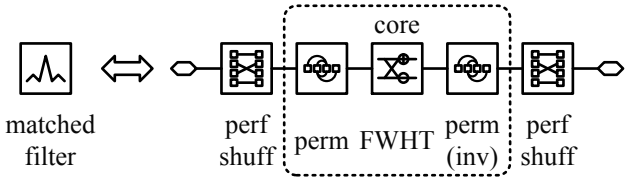

Fig. 5. Matched filter implementation.

C. Antenna model

Another important aspect is a proper representation of the antennas. In the UWB case, they often cause primary signal deformations observable from the receive signal and by this they can affect the range resolution (see [1]). To account for their properties in adequate manner, many literature sources agree, that the (realized) effective length, sometimes also called transfer function, is a suitable characteristic. Based on this characteristic, pole-residue models for different antennas have been reported in [22], which are very conducive for system simulation. Those were derived from frequency domain data of different antenna links using spectral estimation techniques. In our simulations, we use the 4-pole model for a TEM Horn antenna, which is specified in [22] in terms of s-plane poles and residues. From the data given there, we calculated numerator and denominator coefficients for an infinite impulse response (IIR) filter by bilinear approximation. This way, inclusion of the antenna models by use of predefined filter types in ADS Ptolemy is possible.

D. Channel model

Like antennas, the channel might alter signal characteristics as well. In some applications, the impressed channel response is the desired information as it is the case for most medical applications. For other applications, some components might be bothersome, e.g. multipath components in a localization scenario. Here, we use a channel model according to [23], but it should be noted, that there are predefined models for other purposes in ADS as well. According to Fig. 6, the model consists of three components: An attenuator, a delay element and an S-parameter block. Attenuator and delay element account for signal attenuation and retardation in free space. By the S-parameter block, reflectivity of the layered tissuelike model developed in [23] is represented. Frequency behavior of this reflectivity can be traced back to spectral responses of the different dielectric media contained in the layered arrangement which are modeled by multiple Cole-Cole dispersions.

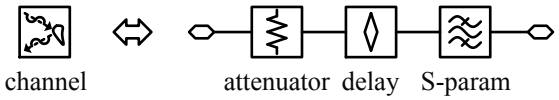

Fig. 6. Channel model.

IV. Simulation Results

A. Signal characteristics

In this subsection, results are discussed, which have been obtained from the setup of Fig. 1. They demonstrate, that access is provided to signal characteristics at relevant system nodes. This knowledge about the signal behavior, which depends on the attributes of applied components, allows further system improvement. In particular, it can be used to optimize the dynamic range of the whole transceiver. In the introduction, this task has been identified to be very conductive for a couple of applications. A prerequisite for such an improvement is precise knowledge about, how components interact and how their characteristics have to be changed to achieve the desired improvement. The basic setup of Fig. 1 and the results of Figs. 7 to 9 can be used as a source for such system tweaking. To achieve the simulation results of Figs. 7 to 9, specifications of components from different system states [24] have been used. Here it is the aim to demonstrate potentials made accessible by system simulation and not the representation of a certain system state.

In Fig. 7, signals are shown as they appear in the transmit path - about $1/8$ of a period is visible. Apart from some smoothing of the signal edges, signals are close to ideal after passing the anti-aliasing filter and the PA. However, the transmit antenna then causes relevant signal deformations (often modeled by signal derivation in a simplifying way). The incident signal at

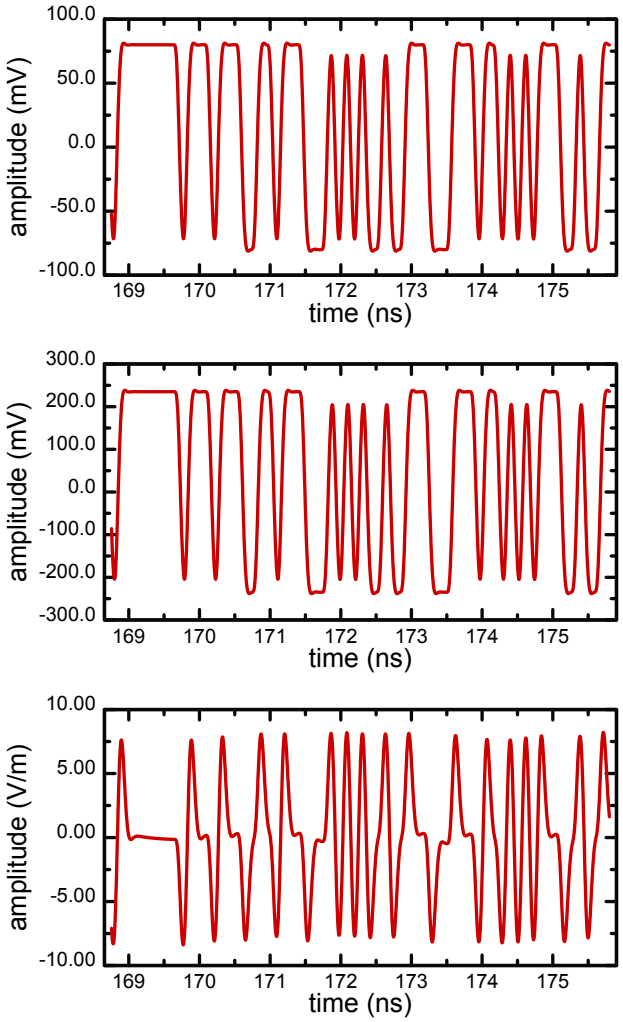

Fig. 7. Signals in the transmit path - from top to bottom: M-sequence processed by the anti-aliasing filter, signal amplified by the PA and signal emitted from the transmit antenna.

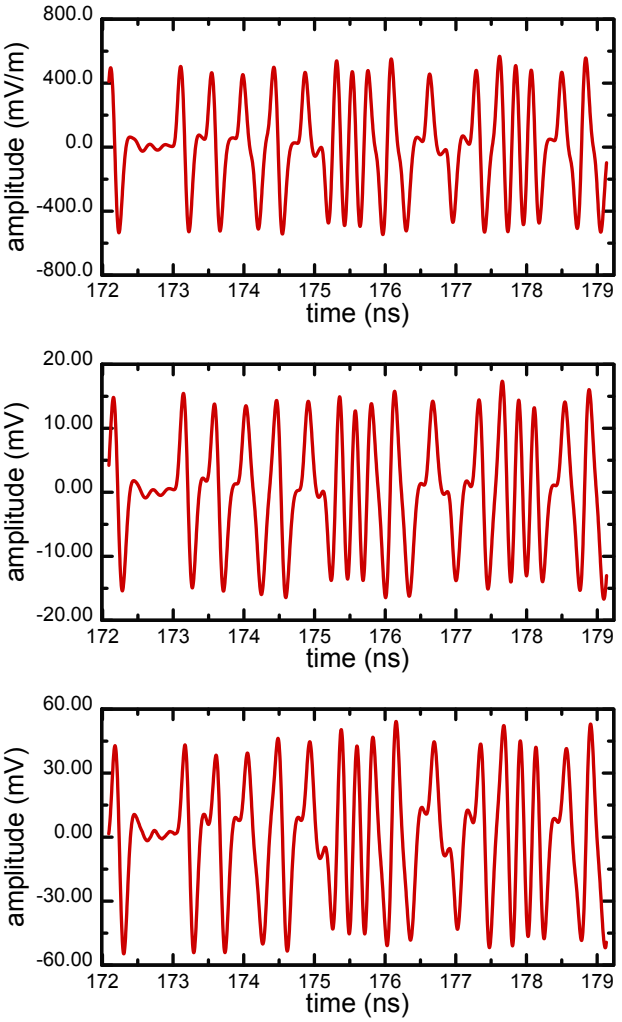

Fig. 8. Signals in receive path - from top to bottom: Signal incident at receive antenna, signal output of receive antenna and signal amplified by LNA.

the receive antenna (Fig. 8 at the top) in addition is influenced by the characteristics of the channel. However, apart from signal inversion, an impact of the channel is barely visible from this plot. The receive antenna itself has only a minor impact on the transient signal shape. Due to AC coupling, the impact of the LNA is a little bit more pronounced, but over all, it basically boosts the receive signal. After discretization, the signal is processed in the digital domain to compute the impulse response function by matched filtering. The result is shown in Fig. 9. As explained in section III, a smooth signal course can be observed due to the application of a (close to) ideal interpolator. This is pronounced by the inset of Fig. 9. Jitter analysis, which is discussed in the next subsection, profits from this additional step. The doublet type impulse response basically arises from the characteristics of the transmit antenna, but also from AC-coupling applied in the LNA. More subtle is the effect of the channel impulse response. It is included in the small side peaks and related

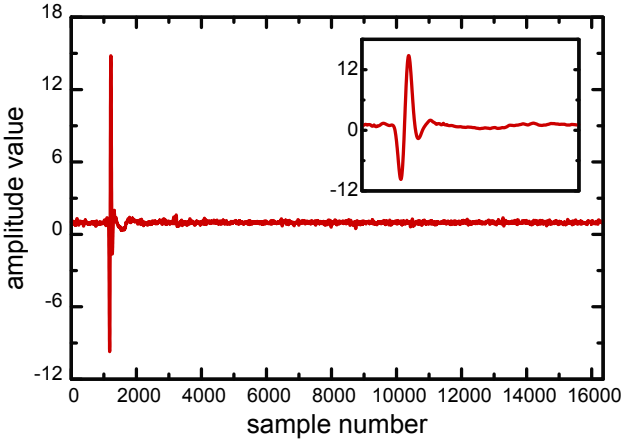

Fig. 9. Impulse response function (IRF) of the system. The inset zooms into the range from $1000 \ldots 2000$. The x-axis is normalized to 4^{th} period.

curve progression. This exemplifies both, the requirement for high dynamic range and low jitter. Simulation of the latter will be analyzed now.

B. Jitter Analysis

As has been noted, IRF jitter is another quantity of special relevance for the system. It arises from random effects like noise, clock and sample time jitter and determines how accurate range measurements can be. In [1] it is shown, that estimates used in narrow band systems are not always optimal for wideband systems and an extended analytical model is proposed. Here, we use an alternative approach. Instead of calculating jitter by analytical expressions, it can be simulated by the setup of Fig. 1. However, in order to save simulation time, we take refuge to one of the results from [1]. While jitter of the clock/trigger system could be included in the simulation by a combination of voltage controlled delay element and noise source, this would require a distinct reduction of the simulation time step, because jitter of this kind is often quite low. Due to the use of steep clock/trigger signals this is especially true for the M-sequence system. Fortunately it is shown in [1], that jitter of the trigger system has only a minor effect on range accuracy in pseudo noise (PN) systems in many cases. Especially, a table is provided, for which it is claimed, that jitter will not provide additional noise if actual jitter caused by an UWB-sensor falls below the indicated values. Therefor, we neglected jitter of the trigger system in our simulations. Also, while Matlab could be invoked from the ADS Ptolemy simulation for the final evaluation, offline processing has been found to be more efficient. Thus, evaluation is only prepared in the simulation and then performed in Matlab. The preparation consists of the interpolation discussed before, because it refines the IRF time course. Hence, it should be eligible to detect threshold crossing by the intercept theorem, i.e. linear interpolation between refined positions. The threshold used is that of the CFAR method proposed in [2]. The algorithm then calculates estimates of the initial delay and the period duration, which is a linear least squares problem. The ideal time positions determined by them finally enable the calculation of rms jitter. Using this approach for evaluation, the result of Fig. 10 could be simulated.
In this figure, IRF jitter or range accuracy for the complete system are displayed versus LNA noise figure, which was swept from $1\,dB$ to $10\,dB$. A single sweep was completed within half an hour on a standard PC work station and yielded 101 IRFs. A single IRF, as presented in the previous subsection, hence can be obtained in a few tens of seconds. During such simulation, the range setting of the channel model was kept at $0.5\,m$.

V. Conclusion

In this paper, we discovered basic requirements, which are common to many UWB sensing problems. Those were related to key figures, which are commonly used for remote sensors. For further examination, we proposed a system simulation setup tied to the M-sequence system at which we focused.

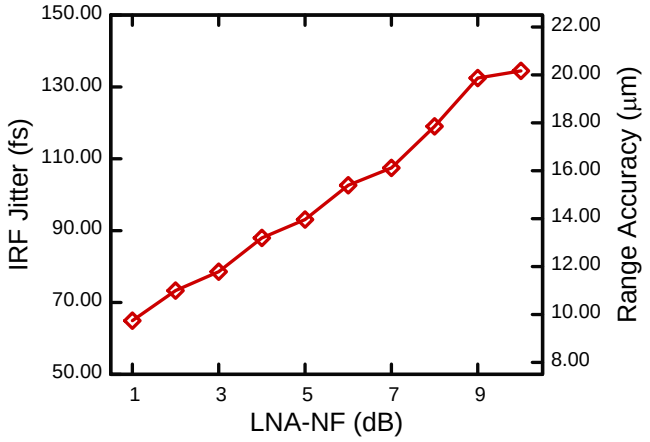

Fig. 10. IRF jitter and range accuracy versus noise figure of the LNA for a distance of $0.5\,m$.

After an in depth treatment of the simulation setup and its constituent components, simulation results have been presented. They show, that proposed setup provides access to signals at relevant system nodes. Especially, a simulation result for the impulse response function was shown. It confirms the requirement of high dynamic range and low jitter. Finally, a jitter analysis based on simulations has been shown, which quantifies the relation of IRF jitter and LNA noise figure. Without system simulation such dependence could not be derived that easy.

Acknowledgment

We would like to acknowledge the German Research Foundation (DFG) for funding this work within the HaLoS project of the UKoLoS framework (SPP 1202). Furthermore, we are grateful to our project partners for years of fruitful collaboration.

References

[1] J. Sachs, M. Helbig, R. Herrmann, M. Kmec, and K. Schilling, "On the range precision of UWB radar sensors," in *11th International Radar Symposium*, Vilnius, Lithuania, Jun.16-18 2010, pp. 1–4.

[2] G. Shen, R. Zetik, H. Yan, O. Hirsch, and R. S. Thomä, "Time of arrival estimation for range-based localization in UWB sensor networks," in *IEEE International Conference on Ultra-Wideband*, vol. 2, Nanjing, China, Sep.20-23 2010, pp. 1–4.

[3] R. Zetik, S. Jovanoska, and R. Thomä, "Simple method for localization of multiple tag-free targets using UWB sensor network," in *IEEE International Conference on Ultra-Wideband*, Bologna, Italy, Sep.14-16 2011, pp. 268–272.

[4] R. Zetik, G. Shen, and R. S. Thomä, "Evaluation of requirements for UWB localization systems in home-entertainment applications," in *International Conference on Indoor Positioning and Indoor Navigation*, Zurich, Switzerland, Sep.15-17 2010, pp. 1–8.

[5] J. Sachs, M. Kmec, R. Herrmann, K. Schilling, R. Zetik, and P. Rauschenbach, "Ultra-wideband pseudo-noise radar: Principle of function, state of the art, applications," in *Sensors and Electronics Panel Specialists' Meeting*. Toulouse, France: NATO Science and Technology Organization, Oct.27-28 2008. [Online]. Available: http://ftp.rta.nato.int/public/PubFullText/RTO/MP/RTO-MP-SET-120/MP-SET-120-11.doc

[6] F. Thiel, O. Kosch, and F. Seifert, "Ultra-wideband sensors for improved magnetic resonance imaging, cardiovascular monitoring and tumour diagnostics," *Sensors*, vol. 10, no. 12, pp. 10 778–10 802, Dec. 2010. [Online]. Available: http://www.mdpi.com/1424-8220/10/12/10778/pdf

[7] J. Sachs, list of publications. [Online]. Available: http://www.tu-ilmenau.de/en/it-emt/mitarbeiter/ausgabe-mitarbeiter/?user_id=2

[8] F. Thiel, M. Helbig, U. Schwarz, C. Geyer, G. Rimkus, W. A. Kaiser, I. Hilger, M. Hein, J. Sachs, and F. Seifert, "Implementation of ultra-wideband sensors for biomedical applications," *Frequenz*, vol. 63, no. 9-10, pp. 221–224, Sep./Oct. 2009. [Online]. Available: http://www.ptb.de/cms/fileadmin/internet/fachabteilungen/abteilung_8/8.1_medizinische_messtechnik/8.11/8.11mrt/Implementation_of_ultra_wideband_sensors_for_biomedical_applications.pdf

[9] M. Kmec, J. Sachs, P. Peyerl, P. Rauschenbach, R. Thomä, and R. Zetik, "A novel ultra-wideband real-time MIMO channel sounder architecture," in *XXVIIIth General Assembly of International Union of Radio Science*, New Delhi, India, Oct.23-29 2005.

[10] *ADS Ptolemy Simulation*, Agilent Technologies, 395 Page Mill Road, Palo Alto, CA 94304 USA, Sep. 2004.

[11] M. Cohn and A. Lempel, "On fast M-sequence transforms," *IEEE Trans. Inf. Theory*, vol. 23, no. 1, pp. 135–137, Jan. 1977.

[12] J. Sachs, R. Herrmann, M. Kmec, and P. Peyerl, "Modified M-sequence UWB-radar," in *German Microwave Conference*, Karlsruhe, Germany, Mar.28-30 2006.

[13] B. Sewiolo, G. Fischer, and R. Weigel, "A 15GHz bandwidth high efficiency power distributed amplifier for ultra-wideband-applications using a low-cost SiGe BiCMOS technology," in *IEEE Topical Meeting on Silicon Monolithic Integrated Circuits in RF Systems*, San Diego, CA USA, Jan.19-21 2009, pp. 1–4.

[14] M. Robens, R. Wunderlich, and S. Heinen, "UWB LNAs for ground penetrating radar," in *IEEE International Symposium on Circuits and Systems*, Taipei, Taiwan, May24-27 2009, pp. 229–232.

[15] M. Robens, S. Bannwarth, R. Wunderlich, and S. Heinen, "Differential UWB-LNA for M-sequence radar," in *Semiconductor Conference Dresden*, Dresden, Germany, Apr.29-30 2009.

[16] M. Robens, R. Wunderlich, and S. Heinen, "Input amplifier for sensitivity improvement in an M-sequence radar front-end," in *International Conference on Indoor Positioning and Indoor Navigation - Abstract Volume*, Zurich, Switzerland, Sep.15-17 2010, pp. 450–451.

[17] Y. Borokhovych, H. Gustat, and C. Scheytt, "4-bit, 16 GS/s ADC with new parallel reference network," in *IEEE International Conference on Microwaves, Communications, Antennas and Electronic Systems*, Tel Aviv, Israel, Nov.9-11 2009, pp. 1–4.

[18] H. S. Stone, "Parallel processing with the perfect shuffle," *IEEE Trans. Comput.*, vol. C-20, no. 2, pp. 153–161, Feb. 1971.

[19] T. H. Tossavainen, "Fast in-place Walsh-Hadamard transform." [Online]. Available: www.musicdsp.org/showone.php?id=18

[20] B. J. Fino and V. R. Algazi, "Unified matrix treatment of the fast Walsh-Hadamard transform," *IEEE Trans. Comput.*, vol. C-25, no. 11, pp. 1142–1146, Nov. 1976.

[21] Y. A. Geadah and M. J. G. Corinthios, "Natural, dyadic, and sequency order algorithms and processors for the Walsh-Hadamard transform," *IEEE Trans. Comput.*, vol. C-26, no. 5, pp. 435–442, May 1977.

[22] S. Licul, "Ultra-wideband antenna characterization and measurements," Ph.D. dissertation, Faculty of the Virginia Polytechnic Institute and State University, Blacksburg, Virginia, Sep. 2004.

[23] F. Thiel and F. Seifert, "Noninvasive probing of the human body with electromagnetic pulses: Modeling of the signal path," *J. Appl. Phys.*, vol. 105, no. 4, Jan. 2009.

[24] R. S. Thomä, H.-I. Willms, T. Zwick, R. Knöchel, and J. Sachs, Eds., *UKoLoS Ultra-Wideband Radio Technologies for Communications, Localization and Sensor Applications*. InTech, 2012, ch. 15, to be published.